



# Numerical Experimental Study on Ore Dilution in Sublevel Caving Mining

Kunpeng Yu<sup>1</sup> · Chunshan Zheng<sup>2,3</sup> · Fengyu Ren<sup>1</sup>

Received: 19 July 2020 / Accepted: 13 October 2020 / Published online: 21 October 2020  
© Society for Mining, Metallurgy & Exploration Inc. 2020

## Abstract

On the basis of physical ore-drawing test research, the irregular particle clusters are constructed by adopting particle element theory and PFC numerical simulation software. Meanwhile, the ore dilution mechanism in the process of stoping caving ore and rock bulk is investigated, especially, the permeability characteristics of small size particles. Main factors considered in the numerical test are particle density ratio, particle diameter ratio, vertical stress of overburden, and shape of large particle size. Results show that the irregular particle morphology could more accurately reflect the permeation characteristics of small size particle in caved ore rocks. The particle diameter ratio and large size particle morphology are significant factors that affect permeability characteristics of caved ore and rock. The infiltration rate and diameter ratio of small particles meet negative exponential function. Meanwhile, the closer the particle size is, the more difficult the infiltration is. In the actual ore-drawing process, the evenness of caving ore-rock bulk should be improved as much as possible, particularly near the ore-rock contact zone.

**Keywords** Ore dilution · Percolation rate · Numerical simulation · Sublevel caving

## 1 Introduction

Sublevel caving is a large-scale underground mining method, which has been widely used in the world since the beginning of twentieth century. This is a top-down mining method that relies on blasting to break the ore and gravity to transport the ore [1, 2]. Ore drawing management is to draw ore according to the prescribed discharge tonnage or grade. The overlying rock mass will naturally collapse as the ore is recovered.

The production process is repeated at multiple subsection levels, a highly mechanized and standardized mining activity [3–6]. The mining and cutting of ore bodies are carried out at different levels, so as to achieve high productivity, high efficiency, and safe working conditions. Compared with other large-scale mining methods, stoping is more flexible and easy

to standardize. This method is simple in structure and has a wide range of application. The mining roadway can be arranged perpendicular to or parallel to the strike of ore body [3]. Sublevel caving is still the main mining method for metal deposits, especially for low-grade mines, and its application will be further expanded.

The main disadvantage of the mining method is the high ore dilution [7–16]. Dilution occurs in the process of ore-drawing, and the contact area between ore and waste rock is large, so the mixing rate of waste rock is high [17–23]. In sublevel caving mining, the ore dilution rate is usually between 15 and 30% [24]. The main reason for low ore recovery is that highly depleted ore is released during ore drawing [25]. The high ore dilution has not been well solved for many years. Main reason is the lack of understanding of the complex relationship between mining parameters and mechanical properties of ore and rock. In the previous studies, most of the attention was paid to the study of single parameters such as stope structure parameters, blasting parameters, and ore-drawing mode, while few studies were made on the comprehensive optimization of multiple parameters in the process of stope mining, thus limiting the further improvement of stope mining index. In this paper, the comprehensive optimization of sublevel caving method is systematically studied by means of physical similarity test and mine field test, combined with the numerical simulation study of PFC software.

✉ Chunshan Zheng  
chunshanzheng@aust.edu.cn

<sup>1</sup> School of Resources and Civil Engineering, Northeastern University, Shenyang 110819, China

<sup>2</sup> State Key Laboratory of Coal Resources and Safe Mining, China University of Mining and Technology, Xuzhou 221116, China

<sup>3</sup> School of Energy and Safety Engineering, Anhui University of Science and Technology, Huainan 232001, China

## 1.1 Numerical Simulation Study

With the development of mining theory and computer technology, many numerical simulation methods have been used to describe the problems in the caving process or to predict the recovery rate of sublevel caving method. Compared with similar test and field test, numerical simulation method is relatively simple and efficient. However, its mathematical model has some limitations, the most important of which is that it is difficult to verify with the actual production data.

Numerical simulation mainly builds models based on finite element method, discrete element method, finite difference method, cellular automata, and empirical analysis [26–28]. With the rapid development of computer technology, the numerical simulation of gravity flow model has risen rapidly in the international mining academia [26–30]. The main numerical simulation methods of ore drawing and corresponding numerical software are introduced as follows.

### 1. Finite element method

Based on the theory of solid plasticity, the finite-element method is used to study the ore-drawing problem by continuous medium particles. The dependence of the loading path of the medium particles was coded into the computer, and a number of scholars studied the vertical stress and the maximum width of the isolated movement zone (IMZ) under different shear strength characteristics of materials [31]. The simulation results of two adjacent drawing points show that when the distance between the drawing points is less than 1.2 times of the maximum width of the IMZ, the non-moving loose body between the drawing points will gradually move. In the field test of Meishan Iron Mine [32], based on the in situ survey, the displacement, and stress monitoring of geological survey, the three-dimensional continuous medium finite element method was used to calculate and study the structural parameters of the large-spacing sublevel caving method. The comparison between the simulation results and the monitoring data shows that when the access spacing distance increases from 15 to 20 m, the stability of studding and stope is significantly improved. For the mining area with poor stability of ore and surrounding rock, increasing the access spacing distance can be beneficial to improve the geo-pressure of stope.

### 2. Cellular automata theory

With the improvement of computing power of computers, it is possible to develop more complex models. Cellular automata theory describes nonlinear phenomena and is an important research method of nonlinear science. Cellular automata are a grid dynamics model with discrete time, space, and state [33]. A cellular consists of a cellular, a state, and a rule. A large number of cells form a dynamic evolutionary system

through simple interactions. The cellular automata model uses partial differential equations to describe the flow of matter in granular media [34–36]. The size and shape of the element body are usually the same, and the flow characteristics of individual particles are determined using probability functions or partial differential equations. Models are usually calibrated according to the results of physical model tests.

Based on cellular automata theory, a large number of scholars have carried out studies on the flow law of caving ore and rock [37, 38]. Sharrock G et al. (2004) [39] developed CAVE-SIM three-dimensional ore drawing numerical simulation software based on cellular automata theory, which can rapidly simulate and analyze the flow process and ore drawing results of caved ore rocks, as well as the visualization of the forms of draw body and IMZ. Castro R et al. (2009) [38] developed a cellular automation flow simulator to simulate ore drawing based on cellular automata model. The cellular automation flow simulator can obtain the spatial position and porosity of medium particles, as well as the shape of draw body and IMZ at different ore-drawing quantities, and can study the ore-drawing problem under different ore-drawing structure, which has the advantages of high calculation efficiency, fast speed, and large scale.

The numerical methods using probability theory to simulate material recovery include discrete element simulation and random simulation. Particles are arranged in a series to simulate their flow, and when a particle is removed, surrounding particles replace it at a user-defined probability. It can simulate the ore-drawing under different structural parameters and solve the problems such as the rule of probability assignment, the assignment of moving probability, the processing of boundary conditions, and the way of stopping ore-drawing. However, these methods do not specify the effect of blasting on the caved rock and deal with the force or rotation of the rock mass. Therefore, there are some limitations in mine drawing simulation by caving method.

### 3. Discrete element method

The assumption that the object of study is composed of a large number of micro-masses connected to each other without gaps does not apply in the field of rock mechanics and mining. In order to correctly evaluate the mechanical properties of rock mass and analyze the flow characteristics of the blasting caved loose mass, a discontinuous medium model needs to be established for research [40, 41]. The discontinuous medium model introduces the actual strength and deformation properties of each structural plane in the mineral rock into the calculation, and studies on the basis of mechanical methods of discontinuous medium, such as discrete element method [42, 43] and discontinuous deformation analysis [43, 44]. Cundall (1971) [41] proposed the discrete element method to analyze the mechanical properties of ore rocks. Cundall,

Strack, and Hart et al. [45, 46] extended their research scope to the study of the mechanical properties of soil and elaborated the idea of discrete element method. The discrete element method combines the physical properties of contact forces and interactions of granular media to establish particle flow models [47–50]. The model captures the displacement, velocity, rotation, and other behaviors of discontinuous particles, as well as the normal and shear forces acting on a single particle [15].

Discrete element method can be divided into microscopic discrete element method and macroscopic discrete element method. The microscopic discrete element method mainly considers the problem of large quantity and discontinuous contact point (contact surface), and analyzes the characteristics of ore-rock engineering from the mesoscopic level. The representative software is PFC (Particle Flow Code). Cundall PA and Hart R (1992) [46] summarized the previous research results and concluded that the element body in the PFC model could generate finite displacement and rotation, and the PFC was the program of particle discrete element method. The macroscopic discrete element method mainly considers the deformation of the discontinuous surface on a large scale. Its representative software is UDEC (Universal Distinct Element Code).

PFC software is mainly used to study the basic characteristics of rock materials, fracture mechanism, and evolution analysis of rock materials, dynamic response of particles, and other basic problems [51]. The main application scope can be summarized as follows: (1) the shipment and mixing of bulk materials; (2) The compression of powdery and granular materials in the casting industry; (3) Flow of loose material in pipes, boxes, grooves, and hoppers; (4) Mining and ore-drawing: rock fracture, collapse, fragmentation, and flow of caved loose bodies; (5) Fluid-solid coupling problem; (6) Structural seismic response and collapse; (7) Research on basic properties of granular materials and dynamic impact response [52].

The application of PFC software based on discrete element method in ore drawing test is characterized by repeatability, convenience, and flexibility, and the essential analysis and description of the movement law of fractured ore and rock can be carried out, indicating the movement, recovery, and rock mixing of ore [51, 53]. Scholars have made many achievements in the application of PFC software in the field of ore drawing. Hashim [54] studied the influence of particle shape, lump distribution, and other factors on the flow characteristics of small particle size by using PFC 3D based on the study of shear strain in the IMZ and draw body during the quantitative ore-mining process with two-dimensional physical model. Pierce [55] used PFC 3D to study the flow characteristics of small particle size in the process of ore-drawing, and put forward the permeability equation of small particle. Pierce and Cundall et al. [56] conducted numerical simulation

of the ore drawing process based on PFC software and found that the formation and development of the IMZ were mainly controlled by the collapse of the stress arch at the top and the friction between the moving particles and non-moving particles at the boundary, and the maximum width of the IMZ was mainly affected by the shape of the particles. Based on the principle and method of two-dimension particle flow numerical simulation, Wang Lianqing et al. (2007) [57] studied and analyzed the caving law of a natural caving method for nickel copper ore. Wang Peitao et al. [58] used PFC software to conduct numerical simulation of the ore-rock movement law of sublevel caving method and ore loss dilution process, and compared and studied the advantages and disadvantages of two different ore-drawing schemes of plane ore-drawing and elevation ore-drawing. Based on orthogonal numerical simulation and profit factor evaluation function, Hu Jianhua et al. [59] constructed an orthogonal PFC numerical model with four factors and three levels, including path spacing, section height, hole angle of collapse edge, and cut-off dilution rate. The optimal parameter combination is determined. It is pointed out that reducing the structural parameters of stope and adopting the management method of low dilution ore-drawing are beneficial to improve the recovery rate of ore-mining of gently inclined medium thick ore-body. Li Bin [60] applied PFC software to study the numerical simulation of single section and single access caving method for ore drawing. Based on PFC software, Zhang Weiyuan and Cheng Aiping [61] conducted a numerical simulation study on low-dilution ore-drawing based on the problem of high ore dilution rate in Shouyun Iron Mine and Jinshan Dian Iron mine respectively, and proved the feasibility of low-dilution ore-drawing method. Xu Shuai et al. [62] used PFC software to conduct numerical simulation research on the flow law of ore and rock mass in steep and thin orebody caving, optimized stope structure parameters, and proposed measures to reduce ore loss and dilution. An Long et al. [63] based on the actual geological conditions and physical properties of ore rocks in Meishan Iron Mine, combined with similar material test and PFC numerical simulation study, carried out the optimization study on the ring spacing of large structural parameters. Lorig and Cundall [64] developed the Rapid Emulator Based on PFC (REBOP) software based on the PFC numerical simulation of ore drawing. A series of equations obtained by REBOP based on PFC simulation results reflect and determine the migration mechanism of caved ore and rock, rather than simulate the process of particle flow [65]. Hancock and Weatherley et al. [66, 67] developed the discrete element method software ESyS-Particle to simulate mining. Based on the calculation of supercomputer, it can simulate the mining model of caving ore and rock up to 200 m, with the number of particles reaching millions.

As for the ore dilution in advance caused by the small size particle migration of the surrounding rock in the process of

drawing, prior work mainly starts from the non-uniformity of broken ore and rock, and it is considered that the ore drawing process is a pulsating process in which the mechanical balance and instability of granular materials alternate. It is concluded that the penetration velocity of fine particles in non-uniform ore-rock dispersion is directly proportional to the total height of ore-rock and inversely proportional to the height of ore layer. The segregation of particles and the penetration of fine particles in field and laboratory tests were preliminarily explained.

Ellipsoid ore drawing theory, random medium ore drawing theory, class ellipsoid ore drawing theory, and computer numerical simulation of flow law of caving and the theoretical study of drawing are depending on the ore and rock medium for uniform continuous flow, does not take into account some heterogeneity of ore in ore. The effect of nonuniformity of caved ore and rock on the drawing process is not considered. At present, there are few researches on ore early dilution caused by the penetration of fine waste rock particles during ore drawing. So a lot of researches are still needed in this area. In the actual production process, the caved ore and rock particles in stope are all non-uniform and the size of the fragmentation is very different. The spatial arrangement of caved ore and rock particles is extremely irregular and the spatial distribution of particles is also extremely uneven. This has a great influence on the flow regularity of the broken ore and rock in the process of ore-drawing. Therefore, in order to make the existing ore-drawing theory conform to the in situ ore-drawing process better, the effect of non-uniformity of ore-rock must be considered. According to the experimental results, measures are proposed to reduce the ore dilution in advance caused by the penetration of fine particles of waste rock.

## 2 Numerical Study on Ore Dilution

The theoretical basis of Particle Flow Code (PFC) software is the microscopic discrete unit theory. Newton's second law is adopted to reflect the complex mechanical behavior of medium. Relationship between particle motion and the force causing the motion is established. The medium particle assembly is discretized into independent units. Newton's second law is repeatedly applied to update the particle motion. The law of cohesion and displacement is used to establish the equations of motion for each discrete element. The explicit central difference method is used to solve the equation according to the cyclic algorithm. It is mainly used to study the basic characteristics of rock materials, the fracture mechanism and evolution law of rock medium, the dynamic response of granular materials, and other basic problems. PFC software is characterized by a finite displacement, rotation, and even complete separation between particles. It can simulate a series of problems in a dynamic process. The ore becomes loose particle

flow after blasting, so the numerical simulation method is suitable for studying the ore-drawing problems such as the flow characteristics of caved ore and rock.

This paper is based on the physical experiment of ore drawing. Based on PFC software, the numerical model of ore drawing is established. The optimal combination of mechanical parameters was determined by comparing the results of the numerical test and physical test. On this basis, the mechanism of ore dilution in the process of ore-rock bulk extraction is explored through the study of the permeability characteristics of small size particles.

### 2.1 Introduction to Basic Theory

Based on the discrete element method, PFC software can simulate the movement and interaction of different spherical particles. The basic function can define the properties of particles, the interactions between particles, and the interactions generated by various boundary conditions.

PFC software uses rigid circles (PFC2D) or spheres (PFC3D) to simulate discrete entities. There are two basic types of contact in the software: particle-particle contact and particle-wall contact. The contact types interact with each other through the force at the contact points, and contact occurs when they move relative to each other and generate the force. The time step algorithm is used to calculate the cycle of the software, and the motion equation cycle is applied to each particle. At the beginning of each time step, the contact settings are updated according to the known particle and wall displacement. The velocity and position of the particle are then updated according to the contact force on the particle and the resultant force and torque on the particle. The wall position is constantly updated with the wall speed [68, 69].

#### 2.1.1 Contact Force Calculation

The normal contact forces of particle-particle contact and particle-wall contact are calculated according to Hooke's Law:

$$F_i^n = K^n U^n \quad (1)$$

where  $K^n$  is the normal stiffness of the contact point, and the size is determined according to the current contact stiffness model.  $U^n$  is the relative normal displacement at the contact point, which satisfies the equation:

$$U^n = \begin{cases} R^{[A]} + R^{[B]} - d, & (\text{Particle-particle}) \\ R^{[B]} - d, & (\text{Particle-wall}) \end{cases} \quad (2)$$

where  $A$  and  $B$  represent particles.  $R^{[A]}$  is the radius of particle  $A$ .  $R^{[B]}$  is the radius of particle  $B$ .  $d$  is the distance from particle to particle or from particle to wall.

Distance  $d$  from particle to particle contact can be obtained from the following formula:

$$d = \left| x_i^{[B]} - x_i^{[A]} \right| = \sqrt{\left( x_i^{[B]} - x_i^{[A]} \right) \left( x_i^{[B]} - x_i^{[A]} \right)} \quad (3)$$

Distance  $d$  from particle-wall contact is determined according to the spatial position relationship between the particle and the wall.

The tangential contact forces of particle-particle contact and particle-wall contact are related to the loading path of the particle movement and shear force on the particle. They are calculated according to the following formula:

$$\Delta F_i^s = -k^s \Delta U_i^s \quad (4)$$

where  $\Delta F_i^s$  is the increment of tangential contact force.  $k^s$  is the normal stiffness of the contact point, which is determined by the contact stiffness model.

### 2.1.2 Particle Bonding Model

If there is a bonding relationship between particles, a number of particles should be bonded together to form a particle cluster [70]. Particle clusters can be used to simulate complex granular morphology, intact rock samples, and uneven boundaries [71]. As shown in Fig. 1, PFC provides two bonding models, parallel bonding model (a) and contact bonding model (b) [72].

As shown in Fig. 1 (a), the parallel bonding model simulates the adhesive gelling material between two adjacent particles, or the elastic beam between two adjacent particles that binds each other [72]. The finite stiffness of the bonding model is in parallel with the stiffness of the contact point. The additional load acting on the particle is assigned to the contact spring and the parallel bonding spring, transmitting forces, and torques. As shown in Fig. 1 (b), the contact bonding model simulates that contact between particles occurs only through a point, and when the normal (or tangential) force is greater than the corresponding bonding strength, the bonding

will break. Point contact bonding transmits only force and does not transmit torque.

According to beam bearing analysis and particle element theory, the maximum tensile stress and the maximum shear stress distributed around the parallel bond are:

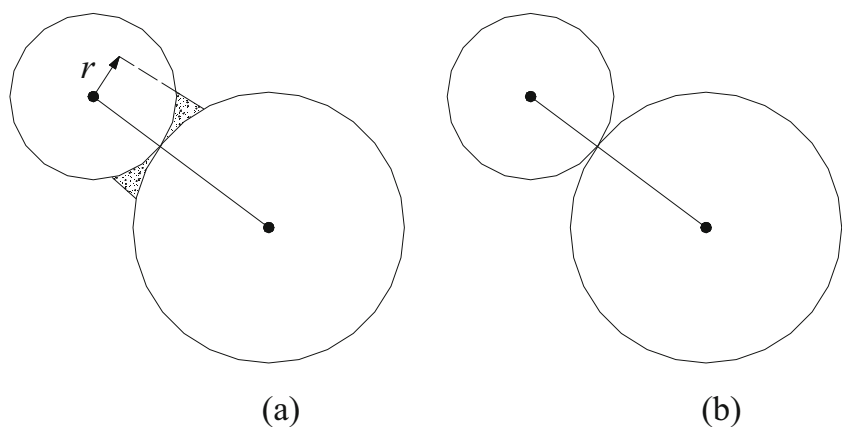
$$\sigma_{\max} = \frac{-\bar{F}^n}{A} + \frac{\left| \bar{M}_i^s \right|}{I} \bar{R} \quad (5)$$

$$\tau_{\max} = \frac{\left| \bar{F}_i^s \right|}{A} + \frac{\left| \bar{M}_i^n \right|}{J} \bar{R} \quad (6)$$

where  $\bar{F}_i$  and  $\bar{M}_i$  are the forces and torques of the parallel bonding model respectively.  $A$  is the cross-section area of the parallel bonding surface.  $J$  is the polar moment of inertia of the section.  $i$  is the moment of inertia of the section along the rotation direction of the contact point.  $\bar{R}$  is the parallel bonding radius, which is equal to the smaller radius in particle  $A$  and particle  $B$  multiplied by the parallel bonding radius coefficient. If the maximum tensile stress exceeds the normal strength, or the maximum shear stress exceeds the tangential strength, then the parallel bonding will fail and the particle state will revert to the current contact stiffness model.

PFC provides two contact stiffness models. They are the simplified Hertz-Mindlin model and the linear model respectively. There is also a rolling impedance contact model [68, 72]. The Hertz-Mindlin simplified model is mainly applicable to the simulation of small deformation and compression, such as the study of wave propagation characteristics in sand and soil under compression. The linear model is mainly used to simulate most of the mechanical behavior in geotechnical engineering. The rolling impedance contact model is mainly applicable to simulate the effect of the actual particle irregular shape, such as the restriction on the dispersion rolling and related energy consumption caused by the asphericity or surface roughness of the contact point [73–76].

Fig. 1 a, b Commonly used bonding model



### 2.1.3 The Boundary Conditions

The function of boundary conditions is to promote the occurrence of various behaviors and act as a store or input of energy [72]. In PFC numerical simulation software, the boundary conditions mainly include gravity, damping, wall, and time step.

#### 1. Gravity and damping force

PFC numerical software exerts gravity by assigning gravity acceleration to each particle. The wall that is exposed to the particles will produce the opposite reaction to the direction of gravity. Therefore, the particle will gradually stabilize the equilibrium state in the process of gravity. In the whole numerical test, gravity is the driving force of particle movement.

Energy conservation is the basic law that numerical simulation models must follow. The effect of damping force in numerical simulation is to maintain the stability and conservation of the numerical model. In the process of the actual particle flow, the kinetic energy will be converted into other forms of energy due to the interaction between the particles and the rupture of the particles. The damping is used to simulate partial energy transfer. On the other hand, with the increase of the calculation quantity of the model, the reduction of the rounder in the finite decimal position of the data calculation is increased, and the large disturbance is produced, and the introduction of the damping can help reduce this disturbance and maintain the stability of the numerical model.

#### 2. Wall

The wall in PFC numerical software is a plane that interacts with particles and has definable contact properties. There are two kinds of walls in the software, the finite wall and the infinite wall. The finite wall is a plane polygon connected together, and the infinite wall is an infinite plane. The main function of the wall is to restrict and restrict the particles in a specific area, and meet the requirements of different boundary conditions through the assignment of parameters such as stiffness, friction coefficient, and contact model.

#### 3. Time stepping

PFC software uses time stepping algorithm to calculate the positions of particles and walls, and the disturbance range in each time step is limited to adjacent units, thus ensuring the accuracy of calculation [52]. The size of a time step is equal to  $\sqrt{(m/k)}$ , where  $m$  represents the mass of the smallest particle in the model and  $k$  represents the maximum stiffness of all particles and walls in the model. The latest version of PFC (PFC 5.0) has added the function of automatic multi-thread

calculation, which realizes the multi-thread calculation of all calculation parts, including the calculation of time step.

## 3 Study on the Seepage Characteristics of Small Size Particle

In sublevel caving, the broken ore is blasted beneath the rock overburden. It is wrapped in the caving surrounding rock and released from the drawpoint. When there are fine particles in the surrounding rock or overburden with a particle size smaller than the gap of the ore dispersion, these fine particles will pass through the ore dispersion in the form of dominant flow and be released from the drawpoint in advance. This phenomenon was also confirmed in the observation of the drawpoint of the test mine, as shown in Fig. 2. Seepage refers to the phenomenon that fine particles pass through the larger particle size layer under the action of gravity and tangential force and have dominant migration (downward movement) [76, 77]. The seepage of silty or small particle size ore and rock is a common phenomenon in the stage of ore recovery [78–80].

The phenomenon of seepage causes the intermingling between different strata of ore and rock, which affects the migration rule of ore and rock in the process of ore-drawing. Then it affects ore recovery and dilution rate. Therefore, it is of great significance to study the characteristics of small particle size dispersion in order to improve the economic benefit of mine and improve the theory and technology of ore drawing. Based on the characteristics of PFC numerical software, it is convenient and quick to use PFC software to study the permeability of small particle dispersion, which is an important method to study this problem.

Bridgwater J et al. [81] conducted shear tests on a large number of spherical particles and obtained that the infiltration rate  $p$  (dimensionless parameter) and the particle size ratio  $d_s/d_l$  (the ratio of small particle size  $d_s$  to large particle size  $d_l$ ) satisfied the following relationship:



Fig. 2 The powder rock (ore) enters the drawpoint

$$p = \frac{L_p}{\gamma_t d_l} = k_1 \exp\left(-k_2 \frac{d_s}{d_l}\right) \tag{7}$$

where  $k_1$  and  $k_2$  are constants.  $L_p$  is the average infiltration distance of small particle.  $\gamma_t$  is the total shear strain.

During ore-drawing, the shear strain will be generated inside the medium units of different heights due to the presence of shear stress, and the relationship between the shear strain  $\gamma$  and the maximum shear angle  $\theta_m$  is [54]:

$$\gamma = \tan\theta_m \tag{8}$$

So the shear strain of the medium element can be calculated by the maximum shear angle.

Therefore, the numerical test obtained the total shear strain required to calculate the seepage rate by controlling the maximum shear angle. By measuring the average infiltration distance of small particle, the infiltration rate  $p$  was obtained. The infiltration rate  $p$  reflects the infiltration characteristics of small particle dispersion.

### 3.1 Numerical Test Design

In this numerical test on the permeability characteristics of small particle dispersion, the following main influencing factors were considered [81]: the density ratio of small particle to large particle  $\frac{\rho_s}{\rho_l}$ , the diameter ratio of small particle to large particle  $\frac{d_s}{d_l}$ , the vertical stress of overburden on the draw body  $\sigma_v$ , and the morphology of large particle.

In numerical tests of ore-drawing particle flow, spherical particles (large particle size) are generally selected to simulate medium dispersion [81]. In this test, in order to more truly reflect the shape of caved ore rocks and the influence of granular rocks on the permeability of small size particles, in addition to the use of spherical particles, non-spherical particles generated by CLUMP command in PFC 3D [68] were also added, namely, three particle clusters and four particle clusters, as shown in Fig. 3. Among them, spherical particles simulate spherical large size particle caving dispersion, three

particle clusters simulate fine long type large size particle caving dispersion, and four particle clusters simulate angular large size particle caving dispersion. The volume of spherical particles in the model is equal to that of three-particle clusters and four-particle clusters.

The expression of the vertical stress in the dispersion of the model medium is:

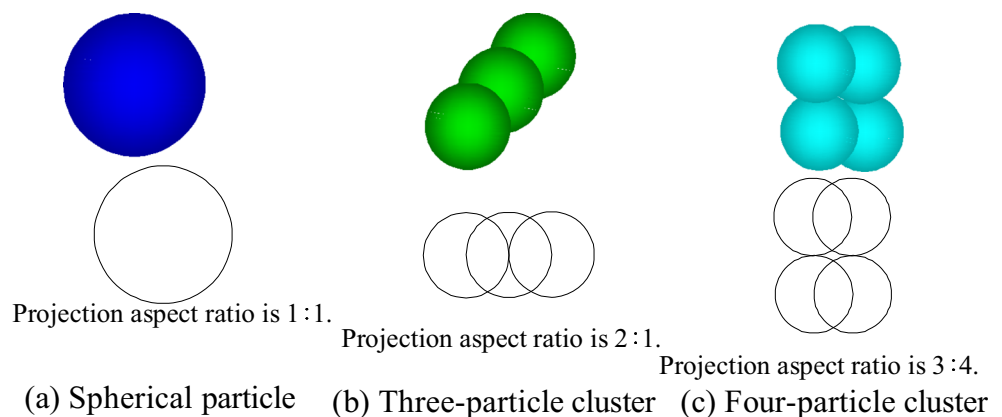
$$\sigma_v = \frac{S\gamma_\rho}{k\tan\phi} \left[ 1 - \exp\left(\frac{-zk\tan\phi}{S}\right) \right] \tag{9}$$

where  $S$  represents the horizontal section area of stope.  $\gamma_\rho$  stands for bulk density of medium.  $k$  represents the friction coefficient between the medium and the wall.  $l$  represents the horizontal section circumference of the stope.  $\phi$  stands for the angle of internal friction of medium dispersion.  $z$  represents the total height of the medium in the model. Apply vertical stress using the PROPERTY command [68] in PFC 3D.

According to the field test results of the blasting fragmentation particle size distribution [69], the average particle size of on-site ore and rock bulk is between 122 and 131 mm, and the fine particle size is < 50 mm. The density of ore and rock loose body after on-site blasting is 5.02 kg/m<sup>3</sup>. The numerical experiment is designed with a geometric similarity ratio of 1:10. Then the values of the four influencing factors are as follows:

1. The density of large-size particles is 5 kg/m<sup>3</sup>, and the density ratio of small-size particles to large-size particles is 0.5, 1.0, and 1.5.
2. The diameter  $d_l$  of large-size particles is 13 mm, and the diameter ratio of small-size particles to large-size particles is 0.2, 0.3, 0.4, 0.5, and 0.6.
3. After repeated debugging, under the condition of 1:10 geometric similarity ratio, the vertical stress of overburden on the released body is calculated as follows: 0.5 kPa, 1.0 kPa, 1.5 kPa.
4. The shape of small size particle is spherical, while the shape of large size particle is spherical, three-particle cluster, and four-particle cluster.

**Fig. 3** The morphology of large particle size in numerical test. **a** Spherical particle. **b** Three-particle cluster. **c** Four-particle cluster



### 3.2 Model Building

The size of the numerical test model is 150 mm in length, 150 mm in width, and 100 mm in height. The actual porosity is taken as the porosity simulated by the particle flow, and the initial porosity is 0.36. The particle is generated by radius expansion method. The intergranular bonding mode was non-bonding model. The specific construction process is as follows:

1. A certain number of large-size particles of specified shape were randomly generated in the area specified by the model, so that the porosity of medium particles was 0.36. In the middle area at the top of the model, 40 small-size particles of specified diameter were randomly generated. The initial positions of small and large particles in the model are shown in Fig. 4. In the model, red particles are small size particle and blue particles are large size particle.
2. Give microscopic mechanical parameters to the wall and particles. Quantitative analysis and suggestions were based on corresponding numerical test results of previous scholars [56, 63, 64]. The optimal micromechanical parameter combination of particles and walls is shown in Table 1. The particle density is the same as the ore density in physical experiment. The coefficient of particle friction is determined according to the natural resting angle of ore-rock dispersion. The friction coefficient of the wall is determined according to the friction coefficient of the inner wall after

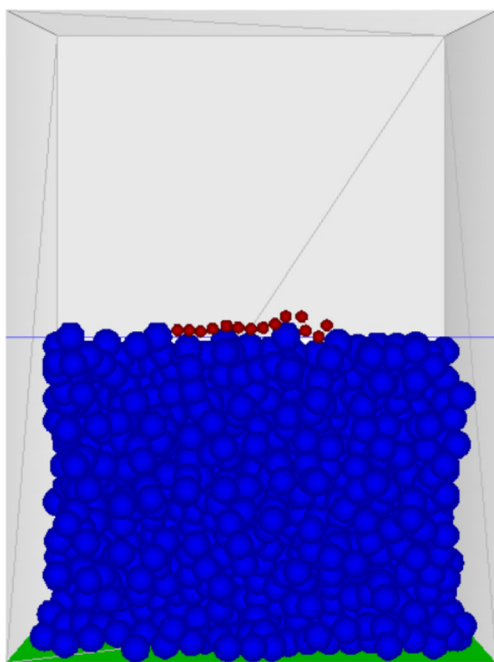


Fig. 4 The initial position of particles in the numerical model

roughening. As for the normal and tangential rigidity of particles and walls, according to the suggestions in literature [63, 64], different values of  $1 \times 10^7$  N/m,  $5 \times 10^7$  N/m,  $1 \times 10^8$  N/m,  $1 \times 10^9$  N/m, and  $5 \times 10^9$  N/m were selected, and the wall stiffness must be greater than the particle stiffness, so as to avoid the wrong result of particles breaking through the wall.

Take the particle’s gravitational acceleration as  $-9.81 \text{ m/s}^2$ . The mechanical parameters shown in Table 1 are assigned to the walls and particles. Corresponding vertical stresses (0.5 kPa, 1.0 kPa, 1.5 kPa) were assigned.

3. Give the left and right sides of the wall a rotation rate of 0.04/s [68]. Rotate in the ①~④ order as shown in Fig. 5. As shown in Fig. 5, the rotation process from ① to ② (or from ③ to ④) causes the corresponding shear strain in the region where the particles are located in the model. The shear strain accumulates until the total shear strain  $\gamma_t$  is reached. Then the permeability of granular particles is calculated. After repeated debugging, the total shear strain  $\gamma_t$  of this numerical test is 190%, and the maximum shear angle  $\theta_m$  is  $26^\circ$ . According to formula (8), the shear strain generated by each step of ①~④ test is  $\gamma = \tan 26^\circ \approx 0.5$ , and the shear strain generated by a complete ①~④ test is  $4 \times \gamma = 4 \times 0.5 \times 100\% = 200\%$ . Then, only one ①~④ rotation is needed to obtain the total shear strain  $\gamma_t$  of 190%.
4. Count the infiltration distance of small particles in the numerical model. Take the infiltration distance of small particle greater than  $5d_l$  (65 mm) from the central area to the wall. In this way, the effect of wall on the infiltration of small particles can be eliminated. The specific method is to call the FISH statement, record the ID of each small size particle at different moments, and visually show the specific position of the small size particle. The particle infiltration distance can be obtained by connecting the vector length of the initial position and the final position of the particle, as shown in Fig. 6. The average permeability distance  $L_p$  of all the small size particles meeting the conditions was

Table 1 Micromechanical parameters of particles and walls

Wall			Particle		
The normal stiffness (N/m)	The tangential stiffness (N/m)	Friction coefficient	The normal stiffness (N/m)	The tangential stiffness (N/m)	Friction coefficient
$1 \times 10^9$	$1 \times 10^9$	0.5	$1 \times 10^8$	$1 \times 10^8$	0.9



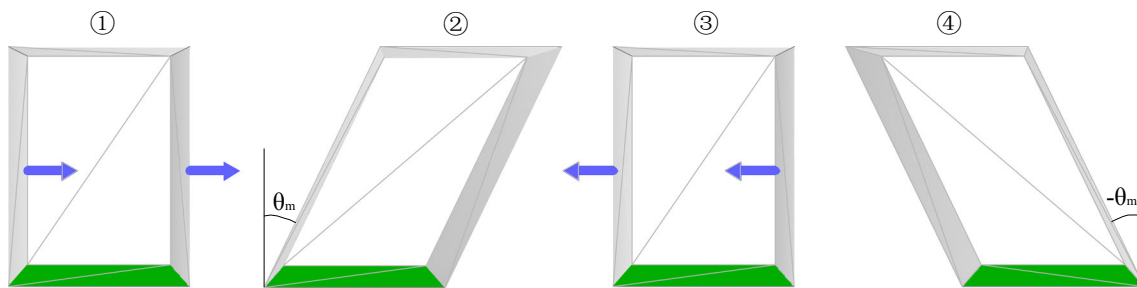


Fig. 5 The rotation process of the wall on both sides of the model

calculated, and the permeability rate of granular particles was obtained by formula (7).

5. The control variable method was used to continue the experiment and the rotation process was repeated (①~④) to obtain the infiltration rate under the influence of four factors (density ratio of small particle to large particle, diameter ratio of small particle to large particle, vertical stress of overburden, and morphology of large particle).

## 4 Analysis of Test Results

### 4.1 Effects of Density Ratio Between Small Size Particle and Large Size Particle on Permeability

Under the condition that the vertical stress of the overburden and the morphology of the large-size particles remain unchanged, the density ratios of the particles are 0.5, 1.0, and 1.5 respectively. The relationship between the infiltration rate of small size particle and the diameter ratio of small size particle and large size particle was obtained. To cover layer of the vertical stress is 0.5 kPa, big size particles for spherical morphology test, for example. The density ratio of the corresponding small particle and large particle was calculated to obtain the relationship between the infiltration rate of small particle and the diameter ratio of small particle and

large particle, and the test data were fitted. The fitting results are shown in Fig. 7.

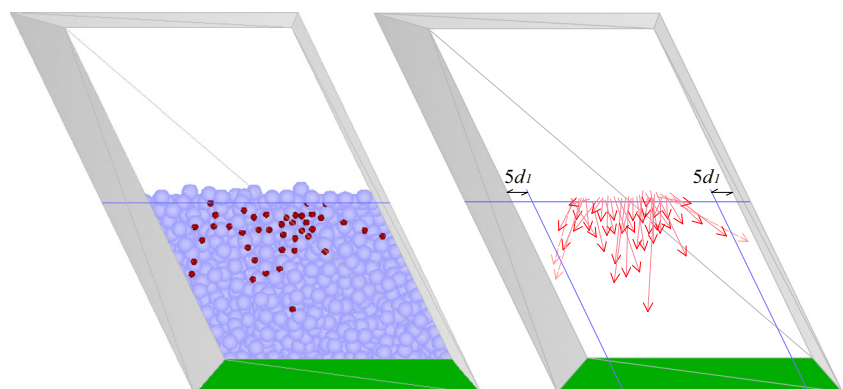
According to the fitting results, when the diameter ratio of small particles and large particles is the same, there is no significant difference in the infiltration rate of small particles corresponding to different particle density ratios, indicating that the density ratio of small particles and large particles has no significant influence on the infiltration rate of small particles.

Similarly, the above tests were repeated with the morphology of large-size particles as three-particle cluster and four-particle cluster respectively, and the experimental data were fitted. The experimental conclusion was that the density ratio of small-size particles and large-size particles had no significant influence on the permeability of small-size particles.

### 4.2 Influence of the Diameter Ratio of Small Particles to Large Particles and the Morphology of Large Particles on the Permeability

Under the condition that the vertical stress of the overburden and the density ratio of small particle size to large particle size are constant, experiments are carried out with different morphologies of large particle respectively to obtain the relationship between the infiltration rate of small particle and the diameter ratio of small size particle to large size particle. For example, the vertical stress of overburden is 0.5 kPa, and the density ratio of small size particle to large size particle is 0.5. The relationship between the infiltration rate of small size particles and the diameter ratio of

Fig. 6 The final state of particles and the displacement of small size particles



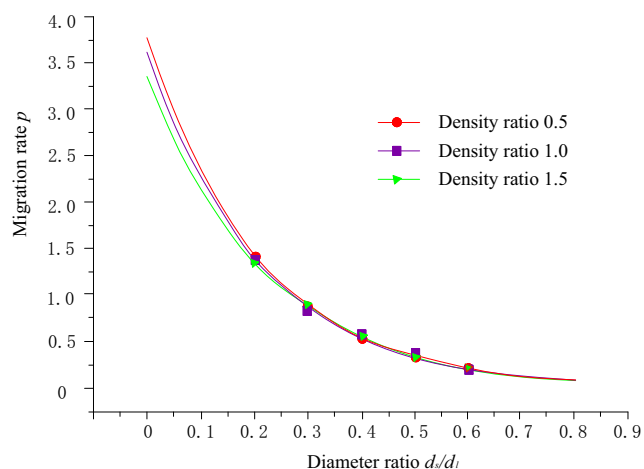


**Fig. 7** The relation between diameter ratio corresponding to different density ratio and infiltration rate

small size particle and large size particle under different large particle morphology was obtained, and the test data were fitted, and the fitting results are shown in Fig. 8.

From the fitting results, it can be seen that when the diameter ratio of small particles and large particles is the same, the infiltration rate of large particles in three and four clusters is significantly lower than that in spherical particles. Three particle clusters represent elongated large-size medium, and four particle clusters represent large-size medium with certain edges and corners. In other words, in the medium with irregular shape (elongated or angular shape), the permeability of small size particle dispersion is weakened.

### 4.3 Influence of Vertical Stress of Overburden on Permeability

The density ratio between small size particle and large size particle and the morphology of large size particle are guaranteed. The control variables were tested with different particle

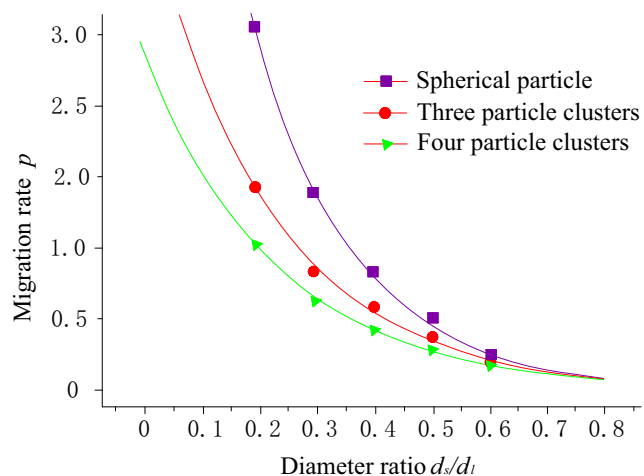


**Fig. 8** The relation between the diameter ratio and permeability of different particle morphology

diameter ratio and vertical stress of overburden. The relationship between the infiltration rate of small size particle and the diameter ratio was obtained. For example, the density ratio of particles is 0.5, and the morphology of large-size particles is three particle clusters. The relationship between the infiltration rate and the diameter ratio of small particles under different vertical overburden stress was obtained. The test data were fitted, and the fitting results are shown in Fig. 9.

From the fitting results, it can be seen that under the condition of the same diameter ratio of particles, there is no significant difference in the infiltration rate of small particles corresponding to the vertical stress of different overburden. In other words, the overburden has no significant effect on the seepage characteristics of small size particles. In other words, the overburden thickness has no significant influence on the seepage of small size particle or silt. Similarly, the above tests were repeated with the shape of large size particle as spherical and four particle clusters respectively, and the test data were fitted. The test conclusion was also that the overburden vertical stress had no significant influence on the seepage characteristics of small size particle.

## 5 Conclusions

In this paper, based on physical ore-drawing test, investigation on the permeability of small size particle is presented. Firstly, particle element theory and PFC numerical software are introduced through contact force, particle, and boundary conditions. By controlling the maximum shear angle, the total shear strain required for seepage rate calculation is obtained. By measuring the average percolation distance of small size particle, the percolation rate can be obtained. Then the percolation rate could reflect the percolation characteristics of small size particle. Main factors to be considered in the numerical test are particle density ratio, particle

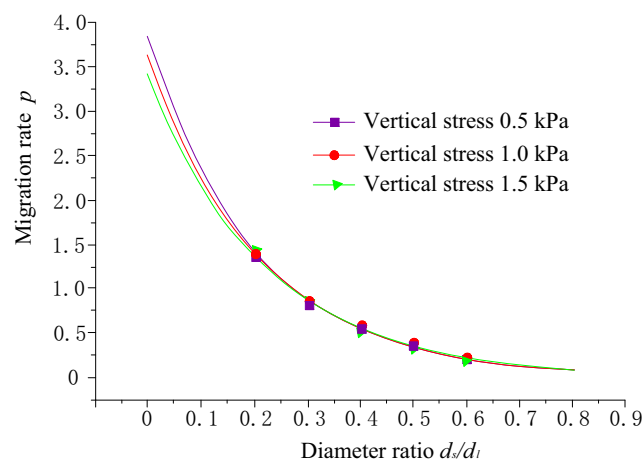


**Fig. 9** The relation between the diameter ratio and permeability of different vertical stresses

diameter ratio, vertical stress of overburden, and shape of large particle size. Following conclusions could be obtained from the numerical test:

1. There is a negative exponential relationship between the diameter ratio of small particle and large particle and the infiltration rate of small particle (Figs. 6, 7, and 8), that is, with the increase in particle diameter ratio, the infiltration rate decreases in the form of negative exponential. Meanwhile, the morphology of large-size particles has a significant influence on the permeability (Fig. 7).
2. The infiltration characteristics of small size particles reflected in this test prove that the shear model based on PFC software has certain practicability in the study of infiltration characteristics.
3. Within the value range of experimental study, the particle diameter ratio and particle size morphology have significant influence on the permeability characteristics, while the particle density ratio and overburden thickness (the vertical stress of overburden on the draw body) have no significant influence on permeability characteristics. The closer the small particle size is to the large particle size, the more difficult it is for small particles to penetrate. The infiltration rate of particles in the spherical medium is obviously higher than that in the medium with irregular shape (long shape and angular shape). In actual ore-drawing, in order to reduce the mixing of waste rock dispersion and delay the early dilution of ore, attention should be paid to improve the uniformity of caving ore and rock dispersion, particularly the uniformity of caving lumpiness near the ore-rock contact surface.

**Funding** This work is financially supported by the National Natural Science Foundation of China (No. 51904013), the Open Research Fund of State Key Laboratory of Coal Resources and Safe Mining, CUMT (No. SKLCRSM20KF003), and the Youth Science and Technology Talents Support Program (2020) by Anhui Association for Science and Technology (No. RCTJ202005).

## Compliance with Ethical Standards

**Conflict of Interest** The authors declare that they have no conflict of interest.

## References

1. Kvapil R (1965) Gravity flow of granular materials in hoppers and bins-Part 2 Coarse material. *Int J Rock Mech Min Sci* 2(3):277–292
2. Alexander DC (2018) Full-scale experiments and numerical modelling to improve ore recovery in sublevel cave mines [D]. University of Queensland
3. Bull G, Page CH (2000) Sublevel caving—today’s dependable low-cost ‘ore factory’ [C]. *MassMin* 2004:537–556
4. Hustrulid W, Kvalip R (2008) Sublevel caving – past and future [C]. 5th International Conference and Exhibition on Mass Mining, Luleå, Sweden: 108–132
5. Janelid I (1972) Study of the gravity flow process in sublevel caving [C]. *International Sublevel Caving Symposium Atlas Copco, Stockholm*, pp 1–23
6. Gertsch RE, Bullock RL (1998) The mechanics and design of sublevel caving s. *Techniques in Underground Mining, Society for Mining, Metallurgy, and Exploration (SME)*: 1
7. Brunton ID, Chitombo GP (2010) Modelling the impact of sublevel caving blast design and performance on recovery [C]. *Rock Fragmentation by Blasting - Proceedings of the 9th International Symposium on Rock Fragmentation by Blasting, FRAGBLAST 9, Granda, Spain*: 353–362
8. Brunton ID, Fraser SJ, Hodgkinson JH, Stewart PC (2010) Parameters influencing full scale sublevel caving material recovery at the Ridgeway gold mine. *Int J Rock Mech Min Sci* 47(4):647–656
9. Janelid I (1968) Sublevel caving: how to use it, what are the advantages, problems. *World Mining* 9:76–78
10. Janelid I (1975) Sublevel caving [C]. *Annual Meeting of the Society of Mining Engineers – AIME* 75: 23
11. Jonsson G (1972) Economic aspects of different layouts and drilling patterns, benefits from reduced dilution and increased recovery [C]. *Sublevel Caving Symposium*: 8
12. Just GD, Free GD (1971) The gravity flow of material in the sublevel caving mining system [C]. *Proceedings of the 1st Australia - New Zealand Conference on Geomechanics, Institution of Engineers*: 88–97
13. Kosowan MI (1999) Design and operational issues for increasing sublevel cave intervals at Stobie mine [D]. *Laurentian University*
14. Mattson R, Cox J (1973) Sublevel caving and draw control procedures and Granduc. *CIM Bull* 4:39–56
15. Wimmer M (2010) Gravity flow of broken rock in sublevel caving (SLC) – state-of-the-art [D]. *Luleå University of Technology, Luleå, Sweden*
16. Zhang G (2004) Behaviour of caved ore mass in sublevel caving and its effect on ore dilution [C]. *4th International Conference and Exhibition on Mass Mining, Chile, Santiago, Chile* 8: 238–242
17. Janelid I, Kvapil R (1966) Sublevel caving. *Int J Rock Mech Min Sci* 3:129–153
18. Just GD (1981) The significance of material flow in mine design and production [C]. *Design and operation of caving and sublevel stoping mines, Society of Mining Engineers – AIME, New York*: 715–28
19. Kvapil R (1982) The mechanics and design of sublevel caving systems [C]. *Underground mining methods handbook, SME, AIM*: 880–897
20. Kvapil R (1992) Sublevel caving in SME mining engineering handbook [C]. *Society for Mining, Metallurgy and Explorations, New York*: 1789–814
21. Power GR (2004) Modelling granular flow in caving mines: large scale physical modelling and full scale experiments [D]. *University of Queensland*
22. Sandstrom P (1972) Application and optimisation of sublevel caving techniques. *Eng Min J* 6:112–125
23. Yenge L (1981) Analysis of bulk flow of materials under gravity caving process – Part 2: Theoretical and physical modelling of gravity flow of broken rock. *Colorado School Mines Q* 73(3):1–67
24. Kvapil R (2004) Gravity flow in sublevel and panel caving - a common sense approach [D]. *Lulea University of Technology, Lulea, Sweden*
25. Kvapil R (1998) The mechanics and design of sublevel caving systems [C]. *Techniques in Underground Mining, Society for Mining, Metallurgy, and Exploration, Inc, Littleton, Colorado*: 621
26. Chitombo GP (2010) Caving mining-16 years after Laubscher’s 1994 paper ‘Cave mining-state of the art’ [C]. *Proceedings of the 2nd International Symposium on Block and Sublevel Caving, Perth*, 45–61

27. Brown ET (2003) Block caving geomechanics [M]. Julius Kruttschnitt Mineral Research Centre, The University of Queensland, Brisbane
28. Yashar P (2013) Mathematical programming for sequence optimization in block cave mining [D]. University of Alberta, Edmonton
29. Jiao J, Qiao CS, Xu GC (2010) Simulation of excavation in numerical manifold method. *Rock Soil Mech* 31(9):2951–2957 (in Chinese)
30. Zheng H, Ge XR, Gu XR et al (1995) Some problems in finite element analysis of geotechnical engineering. *Rock Soil Mech* 16(3):7–12 (in Chinese)
31. Verdugo R, Ubilla J (2004) Geotechnical analysis of gravity flow during block caving [C]. Proceedings of MassMin 2004, Santiago, 195–200
32. Fan JP (2005) Investigation on ground pressure activity law in large spacing nonpillar sublevel caving [D]. Xian:Xi An University of Architecture and Technology. (in Chinese)
33. Zhang XC (2013) Urban geographic information system: Science Press (in Chinese)
34. Castro RL (2006) Study of the mechanisms of gravity flow for block caving [D]. University of Queensland
35. Sharrock G, Hashim M (2009) Disturbed gravity flow in block caving [C]. 43rd US Rock Mechanics Symposium and 4th U.S.-Canada Rock Mechanics Symposium, ARMA Asheville, NC
36. Power GR (2012) Optimizing caving recovery using comparative draw planning strategies and PGCA flow modelling software [C]. MassMin 2012, Sudbury, Canada
37. Deserale D (2002) A versatile two-dimensional cellular automata network for granular flow. *J Appl Math* 62(4):1414–1436
38. Castro R, Gonzalez F, Arancibia E (2009) Development of a gravity flow numerical model for the evaluation of drawpoint spacing for block/panel caving. *J Southern African Inst Mining Metall* 109(7):393–400
39. Sharrock G, Beck D, Booth G, et al (2004) Simulating gravity flow in sub-level caving with cellular automata [C]. Proceedings of MassMin 2004, Santiago, 2004, 189–194
40. Cundall PA (1971) The measurement and analysis of acceleration on rock slopes [D]. London: University of London, Imperial College of Science and Technology
41. Cundall PA (1971) A computer model for simulating progressive large scale movements in blocky rock systems [C]. Proceedings of the International Symposium Rock Fracture, ISRM, Nancy, 1–8
42. Liu SH (2009) Application of discrete element method in rock and soil mechanics [C]. Abstract of papers presented at the Academic Congress of the Chinese Mechanics Society. Zhengzhou University:434. (in Chinese)
43. Wang JY, Xing JB (1995) Discrete element method is the same as Lagrange Yen method and its application in rock and soil mechanics. *Rock Soil Mech* 02:1–14 (in Chinese)
44. Wang JY, Xing JB (1991) Discrete element method and its application in rock and soil mechanics [M]. Shenyang: Northeast Institute of Technology Press. (in Chinese)
45. Cundall PA, Strack ODL (1979) A discrete numerical model for granular assemblies. *Geotechnique* 29(1):47–65
46. Cundall PA, Hart R (1992) Numerical modeling of discontinua. *Eng Comput* 9(2):101–113
47. Shi GH, Pei JM (1997) Numerical manifold method and discontinuous deformation analysis [M]. Beijing: Tsinghua University Press. (in Chinese)
48. Hancock W (2013) Gravity flow of rock in caving mines: numerical modelling of isolated, interactive and non-ideal draw [D]. University of Queensland
49. Minchinton A, Dare-Bryan P (2005) The application of computer modelling for blasting and flow in sublevel caving operations [C]. Ninth Underground Operators' Conference 2005, The Australasian Institute of Mining and Metallurgy: Melbourne: 65–74
50. Sellden H, Pierce M (2004) PFC3D modelling of flow behaviour in sublevel caving [C]. MassMin 2004, University of Santiago, Santiago, Chile: 201–214
51. Zhu HC (2006) PFC and its application in caving mining research. *J Rock Mech Eng* 25(9):1928–1931 (in Chinese)
52. Sun H (2019) Study on the evolutionary mechanism of caving ore and rock migration based on particle element theory [D]. University of Science and Technology Beijing. (in Chinese)
53. Zhang JW (2017) Simulation study on three - dimensional release law of top coal in fully mechanized caving [D]. China University of Mining and Technology (Beijing). (in Chinese)
54. Hashim MHM (2011) Particle percolation in block caving mines [D]. Sydney: The University of New South Wales
55. Pierce ME (2004) PFC3D modeling of inter-particle percolation in caved rock under draw [C]. Numerical Modeling in Micromechanics via Particle Methods-2004, Proceedings of the 2nd International PFC Symposium, Kyoto, 149–156
56. Pierce ME, Cundall PA, Van Hout GJ, et al (2002) PFC3D modeling of caved rock under draw [C]. Proceedings of the 1st International PFC Symposium, Gelsenkirchen, 211–217
57. Wang LQ, Gao Q, Wang JG, Fang ZL (2007) Numerical simulation of particle flow by natural caving mining method. *J Univ Sci Technol Beijing* 06:557–561 (in Chinese)
58. Wang PT, Yang TH, Liu XB (2010) PFC2D numerical simulation of ore drawing rule with pillarless sublevel caving. *Metal Mine* 08:123–127 (in Chinese)
59. Hu JH, Guo FZ, Luo XW, Zhou KP, Ji DB (2015) Simulation of ore flow law and optimization of drawing parameters in caving mining of gently inclined medium thick ore body. *J Central South Univ (Science and Technology)* 46(05):1772–1777 (in Chinese)
60. Li B (2012) Study on drawing regularity and drawing step optimization in Chengchao Iron Mine of Wisco [D]. Wuhan University of Technology. (in Chinese)
61. Zhang WY (2013) Three-dimensional numerical simulation of low dilution ore-drawing [D]. Harbin Institute of Technology. (in Chinese)
62. Xu S, An L, Feng XT, Dong JK, Li YH (2013) Study on flow regularity of ore and rock bulk in steep and thin vein caving. *J Mining Saf Eng* 30(04):512–517 (in Chinese)
63. An L, Xu S, Li YH, Peng JY (2013) Optimization of caving distance based on multi - method. *Chin J Rock Mech Eng* 32(04):754–759 (in Chinese)
64. Lorig LJ, Cundall PA (2000) A rapid gravity flow simulator [R]. Brisbane: JKMRC and Itasca Consulting Group, Inc
65. Carlson G, Tyler D, DeWolfe C, et al (2004) Understanding gravity flow for mix and dilution modeling at Henderson Mine [C]. Proceeding of MassMin 2004, Santiago, 231–237
66. Hancock WR, Weatherley DK (2008) 3D simulations of block caving flow using EsyS-Particle [C]. Proceedings of the 1st Southern Hemisphere International Rock Mechanics Symposium, Perth, 221–229
67. Hancock WR, Weatherley DK, Chitombo GP (2010) Large-scale simulations of gravity flow in block caving [C]. Proceedings of the 2nd International Symposium on Block and Sublevel Caving, Perth, 553–566
68. Itasca CG (2008) User's guide in PFC3D version 4.0 [M]. Minneapolis: Itasca Consulting Group Inc
69. Zhou Y (2014) Analysis technique of discontinuous equivalent rock mass and study on mechanical parameters of meso-weakened jointed rock mass [D]. Beijing: University of Science and Technology Beijing. (in Chinese)
70. Potyondy DO, Cundall PA (2004) A bonded-particle model for rock. *Int J Rock Mech Min Sci* 41:1329–1364
71. Potyondy DO (2014) The bonded-particle model as a tool for rock mechanics and application: current trends and future directions. *Geosyst Eng* 17(6):342–369

72. Itasca CG (2014) User's guide in PFC version 5.0 [M]. Itasca Consulting Group Inc., Minneapolis
73. Sakaguchi H, Ozaki E, Igarashi T (1993) Plugging of the flow of granular materials during the discharge from a soil. *Int J Modern Phys B* 7:1949–1963
74. Zhou YC, Wright BD, Yang RY et al (1990) Rolling friction in the dynamic simulation of sandpile formation. *Physica A* 269:536–553
75. Chang CS, Liao CL (1990) Constitutive relation for a particulate medium with effect of particle rotation. *Int J Solids Struct* 26:437–453
76. Hogg R (2003) Characterization of relative homogeneity in particulate solids. *Int J Miner Process* 72(1–4):477–487
77. Tang P, Puri VM (2004) Methods for minimizing segregation: a review. *Part Sci Technol* 22(4):321–337
78. Li T, Wu AX, Han B et al (2016) Study on the seepage process of fine particles in ore-drawing by natural caving method based on discrete element theory. *J Eng Sci* 3(11):1509–1514
79. Wen YM (2011) Study on control method of ore dilution in overburden [D]. Kunming: Kunming University of Science and Technology. (in Chinese)
80. Li CN (2000) Study on flow regularity and application of non-uniform ore-rock dispersion [D]. Shenyang: Northeastern University. (in Chinese)
81. Bridgwater J, Cooke MH, Scott AM (1978) Inter-particle percolation equipment development and mean percolation velocities. *Trans Inst Chem Eng* 56:157–167

**Publisher's Note** Springer Nature remains neutral with regard to jurisdictional claims in published maps and institutional affiliations.